HHS Public Access

Author manuscript

Mol Pharm. Author manuscript; available in PMC 2021 July 12.

Published in final edited form as:

Mol Pharm. 2019 July 01; 16(7): 3253–3260. doi:10.1021/acs.molpharmaceut.9b00453.

A Biliary Tract-Specific Near-Infrared Fluorescent Dye for Image-Guided Hepatobiliary Surgery

Michael P. Luciano[#†], **Jung-Man Namgoong**[#‡,§], **Roger R. Nani**[†], **So-Hyun Nam**[‡,⊥], **Choonghee Lee**[¶], **Il Hyung Shin**[¶], **Martin J. Schnermann**[*,†], **Jaepyeong Cha**[*,†,#]

[†]Chemical Biology Laboratory, Center for Cancer Research, National Cancer Institute, 376 Boyles Street, Frederick, Maryland 21702, United States

[‡]Sheikh Zayed Institute for Pediatric Surgical Innovation, Children's National Health System, 111 Michigan Avenue Northwest, Washington, D.C. 20010, United States

[§]Department of Surgery, University of Ulsan College of Medicine, Asan Medical Center, 88 Olympic-ro, 43-gil, Songpa-gu, Seoul 138-736, South Korea

[⊥]Department of Surgery, Dong-A University College of Medicine, 26 Daesingongwon-Ro, Seo-Gu, Busan 49201, South Korea

[¶]InTheSmart Co, Center for Medical Innovation Bld, 71 Daehak-ro, Jongro-gu, Seoul, South Korea

[#]Department of Pediatrics, George Washington University School of Medicine and Health Sciences, 2300 Eye Street Northwest, Washington, D.C. 20052, United States

[#] These authors contributed equally to this work.

Abstract

Despite advances, visual inspection, palpation, and intraoperative ultrasound remain the most utilized tools during surgery today. A particularly challenging issue is the identification of the biliary system due to its complex architecture partially embedded within the liver. Fluorescence guided surgical interventions, particularly using near-infrared (NIR) wavelengths, are an emerging approach for the real-time assessment of the hepatobiliary system. However, existing fluorophores, such as the FDA-approved indocyanine green (ICG), have significant limitations for rapid and selective visualization of bile duct anatomy. Here we report a novel NIR fluorophore, BL (Bile Label)-760, which is exclusively metabolized by the liver providing high signal in the biliary system shortly after intravenous administration. This molecule was identified by first screening a small set of known heptamethine cyanines including clinically utilized agents. After finding that none of these were well-suited, we then designed and tested a small series of novel dyes within a

[*]**Corresponding Authors** martin.schnermann@nih.gov.; jcha2@Childrensnational.org.

Supporting Information

The Supporting Information is available free of charge on the ACS Publications website at DOI: 10.1021/acs.molpharmaceut.9b00453.

Synthetic procedures and NMR data (PDF)

The authors declare the following competing financial interest(s): Dr. Namgoong, Dr. Luciano, and Dr. Nam have no conflict of interest to disclose. Dr. Nani, Dr. Schnermann, and Dr. Cha have a patent pending on the fluorescent dye, US 62/631,390. Dr. Lee and Dr. Shin were employed by InTheSmart USA Incorporated, when the research was carried out. Dr. Shin has ownership interest to InTheSmart USA Incorporated. Non-institutional funding was provided by InTheSmart Incorporated, USA.

prescribed polarity range. We validated the molecule that emerged from these efforts, BL-760, through animal studies using both rodent and swine models employing a clinically applicable imaging system. In contrast to ICG, BL-760 fluorescence revealed a high target-to-background ratio (TBR) of the cystic duct relative to liver parenchyma 5 min after intravenous injection. During hepatic resection surgery, intrahepatic ducts were clearly highlighted, and bile leakage was easily detected. In conclusion, BL-760 has highly promising properties for intraoperative navigation during hepatobiliary surgery.

Graphical Abstract

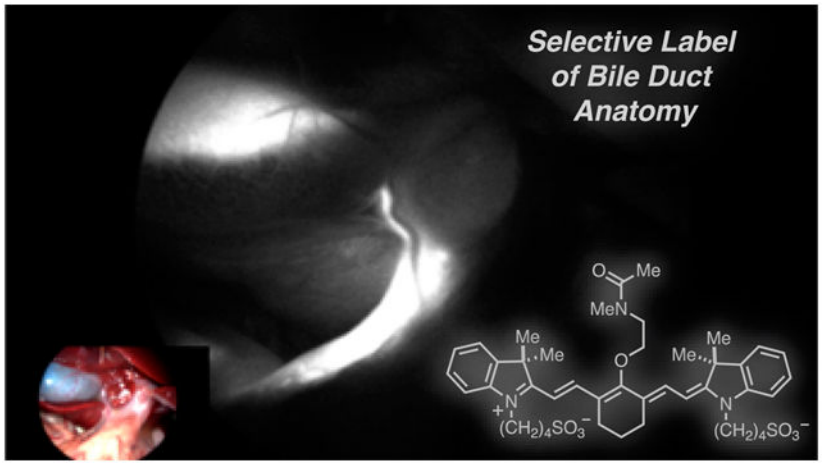

Keywords

heptamethine cyanine; near-infrared fluorescence; hepatobiliary surgery; bile duct; fluorescence laparoscopy

INTRODUCTION

The identification and preservation of critical anatomical structures are key to successful surgical outcomes.[1] The hepatobiliary tract is regarded as one of the most difficult anatomical features to distinguish from neighboring tissues. Unrecognized injuries to the bile duct can result in debilitating short- and long-term morbidity, mortality, and healthcare burdens.[2] Bile duct injuries can occur intraoperatively and are more common under conditions of severe inflammation, adhesion, or unexpected anatomical variations.[3-5] Additionally, emerging minimally invasive methods make precise anatomical identification more difficult due to impaired tactile sensation.[6,7] Consequently, methods that enable intraoperative display of bile duct anatomy are of paramount importance for the prevention of iatrogenic injury.

Currently, bile duct visualization methods include intraoperative cholangiography, which can be used to impart significant situational awareness.[8] In particular, detailed division of the biliary tract during living donor hepatectomy for liver transplantation is crucial both for donor safety and graft function.[9,10] However, in some cases, cholangiography itself does not

provide enough information because of insufficient contrast from the injected radioactive tracer and heavily overlapping surrounding tissues. In fact, recent literature questions the advantages of routine cholangiography.[11] Furthermore, intraoperative cholangiography is time-consuming, and the introduction of a catheter into the common bile duct (CBD) can induce leakage.[12] Laparoscopic ultrasonography is a less invasive method to identify CBD stones and anatomical abnormalities, but this technique has not been deployed broadly.[13]

Fluorescence guided surgical (FGS) methods, especially those using near-infrared (NIR) wavelengths, are rapidly emerging. Significantly, the recent progress in translation of these approaches has demonstrated that novel agents can progress into exploratory and, likely soon, routine clinical use.[14-16] NIR-FGS using indocyanine green (ICG) has recently been reported as an alternative to conventional cholangiography. Such methods have been used to assist in the identification of the bile duct in cholecystectomy and for bile leakage imaging during hepatectomy.[17-21] However, because the ICG signal persists in the liver parenchyma for up to 240 min postinjection, timing the injection to achieve useful contrast is quite challenging.[22] Ideally, high-contrast signal would be achieved within minutes to allow the surgeon to administer the dye only once there is a medical need for anatomical reference. Several studies also reported retrograde injection of a NIR probe directly into the bile duct; however, the introduction of a catheter could result in iatrogenic damage.[23,24] Other studies have proposed using methylene blue (MB), which undergoes rapid biliary excretion into bile. However, the emission maximum of MB is 700 nm rather than 800 nm, which is suboptimal from both an instrumentation and scattering/absorption standpoint.[25] Therefore, there remains an unmet clinical need for NIR fluorescent markers characterized by rapid biliary-specific excretion and sustained high contrast relative to the adjacent liver tissue.

Here we report a novel heptamethine cyanine, BL-760, for use as a fluorescent marker of the biliary tract. To identify this compound, we first examined known dyes including those already used in a clinical setting. After finding that these molecules were not well suited, a small library of related C4′-*O*-alkyl heptamethine cyanine analogs of intermediate polarity were designed and synthesized. Initial testing in an open-abdomen model of rat surgery revealed the optimal compound, BL-760, which was almost exclusively taken up by the liver and rapidly excreted into the bile tract. This compound produces a rapid onset of fluorescent signal exclusive in the bile duct (5 min), signal persistence (>3 h), and no discernible toxicity. Advantageously, this molecule can be synthesized in two steps from commercial IR-783, a readily available chemical precursor. We then validated BL-760 *in vivo* through preclinical animal studies using both rodent studies and a swine hepatectomy model, with the latter employing a laparoscopic commercial fluorescence imaging system already approved for clinical use.

MATERIALS AND METHODS

Synthesis and Characterization.

The synthetic procedures are described in detail in the Supporting Information. The absorbance and fluorescence of BL-760 were measured as described previously.[26] Fluorescence quantum yield (QY) measurements were carried out using ICG in MeOH (QY = 7.8%) as a calibration standard under conditions of matched absorbance at 770 nm.

Rat Protocol.

Children's National animal care and use committee approved our protocol (IACUC # 30597). All procedures were performed in the Research Animal Facility at Children's National Hospital. Female 250–300 g Sprague–Dawley rats from Charles River Laboratories (Wilmington, Massachusetts, USA) were used for this experiment. Inhalation for 3 min of 4% isoflurane was used for sedation and restraint. Anesthesia was maintained using an intramuscular injection of xylaxine (2 mg/kg) and ketamine (75 mg/kg). After ensuring sterile conditions, a laparotomy was performed. For fluorescence imaging, a 24G catheter was placed in the tail vein and injection of the fluorophore (90 μg/kg) was performed, with immediate imaging after injection.

Pig Protocol.

All procedures were performed in an animal research facility under the approval of the Institutional Animal Care and Use Committee at the Children's National Health System (protocol #30591). To better model a minimally invasive surgery (MIS) experience, we performed laparoscopic imaging in swine. Female Yorkshire pigs (25–30 kg) from Archer Farms (Darling, Maryland, USA) were used for the experiment. The pigs were sedated using an intramuscular injection of xylazine and ketamine, and anesthesia was maintained using 2.5% isoflurane. Midline laparotomy was performed. At the beginning of the procedure (via the so-called, "critical view of safety" approach in Cholecystectomy), Calot's triangle was exposed and imaged. After 2 h of imaging, a left lobectomy was performed using electrocautery (30/30) to visualize the intrahepatic duct alongside the liver parenchyma.

NIR Fluorescence Imaging: Rat Protocol.

To enable both RGB color and fluorescence image recording, an existing surgical microscope OPMI S5 (Karl Zeiss, Germany) with two additional camera ports was used.[26] The microscope includes a 250 mm focal-length main objective lens and two camera ports located on both the left and right arms split by a virtual beamsplitter integrated into the main body of the scope. CAM1 (GS3-U3–41C6C–C, FLIR, U.S.) was used for HD color vision, which operates at 30 frames per second with 2048 × 2048 pixels. CAM2 (GS3-U3–41C6NIR-C, FLIR, U.S.) was used for NIR fluorescence imaging, which included a band-pass filter (790/30 nm) and also operated at 30 frames per second with the same 2048 × 2048 pixels. For illumination, we used a built-in microscope illuminator with a short-pass filter (cutoff wavelength: 800 nm). For simultaneous visualization and recording, all the scripts for camera control were custom built and programmed using a Linux operating machine.

NIR Fluorescence Imaging: Pig Protocol.

For laparoscopic fluorescence imaging, a FDA-cleared commercial fluorescence laparoscopic imaging system was used (ITS Model L, inTheSmart Incorporated, USA). To illuminate the tissue, we used a clinically available (FDA-approved) power-adjustable dual light source (ITSEL1711, InTheSmart Incorporated, USA) consisting of a visible spectrum (400–700 nm) high-power quad-LED and a NIR (810 nm) laser, which share a common optical path.[27] This source is then coupled to the illumination port of the laparoscope via a

fiber-optic light guide cable (ITSEL1711-LGCBL-V01, InTheSmart Incorporated, USA). The power of the visible light and laser sources can be separately controlled on a 0–100% scale in steps of 10%. To ensure tissue safety and prevent pixel saturation, the laser power measured 5 cm from the tip of the laparoscope was set as low as the 50 mW, corresponding to a maximum power setting of 30%.

Intraoperative Imaging and Quantitative Assessment.

For the rat surgeries, a standard midline laparotomy was performed. For fluorescence imaging, a 24G catheter was placed in the tail vein and each compound (90 μg/kg) was administered by injection and then imaged immediately after. The imaging system was set up, and videos were recorded in real time until 3 h after injection of the fluorophore. All images were acquired with a 33 ms exposure time.

For the pig studies, a 0-degree, 10 mm laparoscope was positioned with noga arm (Articulated Holder FAT MA61003, Noga, Israel). The laparoscopic system was set up, and videos were recorded over the 3 h after injection of the fluorophore. The ratio between fluorescence and background signals in a region of interest was quantified using ImageJ software. The target-to-background ratio (TBR) was calculated as follows: TBR = (Target-Noise)/(Background-Noise), where the background was normal adjacent liver parenchymal tissue and the target was the CBD. Noise was used in a region outside the target and background. The results are presented as mean ± standard error of the mean (SEM).

RESULTS AND DISCUSSION

Testing Known Fluorophores.

We initially tested readily accessible fluorophores. These include two NIR fluorophores that have found clinical use, ICG, which is FDA approved, and IR-800CW, which is progressing through various clinical trials as a folate and antibody conjugate.[28-32] We also tested two compounds recently reported for our studies: FNIR-774, a bio-conjugatable dye, and UL-766, a compound that we recently reported as undergoing exceptionally clean renal clearance.[33] Testing involves administration of the fluorophore (90 μg/kg, i.v., $n = 2$) to rats that had undergone a laparotomy, followed by fluorescence imaging of the abdomen using a surgical microscope.

Unfortunately, these compounds showed suboptimal characteristics for use as bile markers. In line with the prior clinical work, ICG exhibits a prolonged signal in the liver parenchyma, and 4 h are required to achieve maximal bile duct signal relative to liver parenchyma. By contrast, IR-800CW undergoes competitive renal and liver clearance. Although some bile duct signal is apparent shortly following injection, so too is significant competitive signal in the kidneys, bladder, and ureter, making this dye suboptimal for selective imaging of bile duct anatomy. FNIR-774, which is similarly persulfonated to IR-800CW, also undergoes competitive clearance through renal and liver pathways. Finally, and in line with our prior work, we found the zwitterionic ureter dye, UL-766, is nearly exclusively cleared through renal means in this comparison.[26]

Design, Synthesis, and Initial Identification of BL-760.

To interpret these patterns of excretion, we examined the total number of charged functional groups, net charge, and a common measure of hydrophilicity, ClogP.[33] As shown in Figure 1, ICG, which is the only molecule to undergo exclusive hepatobiliary-mediated clearance, is significantly more hydrophobic than the persulfonated dyes, IR-800CW and FNIR-774, and the charge-neutral, UL-766. Of note, the hepatic uptake of ICG has been shown to be largely mediated by organic anion transporter polypeptides (OATP) influx transporters and its excretion into the bile involves multidrug resistance P-glycoprotein 2 (Mdr2).[35-37] We hypothesized that anionic heptamethine cyanines of intermediate hydrophilicity between ICG and the extensively persulfonated IR-800CW and FNIR-774 might exhibit improved rates of liver clearance, while maintaining high specificity over renal excretion pathways.

To pursue this hypothesis, we prepared a small series of C4′-*O*-alkyl cyanines based on our prior synthetic approach. This approach involves an *N*-to-*O* transposition reaction that converts readily accessible C4′-*N*-alkyl cyanines into the otherwise difficult to prepare *O*-alkyl derivatives.[32] Advantageously, and unlike extensively studied C4′-*O*-phenol cyanines, *O*-alkyl cyanines are not subject to covalent modification with biomolecules.[33,38,39] The molecules we tested included compound **1**, which had been prepared previously,[30] and compounds **2–4**, which were synthesized in an analogous fashion (see Figure 2A for the general synthetic approach and the Supporting Information for details). The spectroscopic properties for compounds **2–4** were quite similar and in line with previously prepared compounds. Data for a representative compound, **4**, are shown in Figure 2B and C.

As shown in Figure 3, compounds **1–4** all underwent nearly exclusive hepatobiliary clearance. However, compounds **3** and **4** exhibit rapid onset of bile signal (5 min) and that signal persisted for several hours. Because of its slightly simpler chemical structure, compound **4**, now termed BL (Bile Label)-760, was progressed into evaluation in pig models.

Comparison of BL-760 and ICG in Swine Model.

In these studies, both ICG and BL-760 (90 μg/kg, i.v.) were administered, and the fluorescence signals were acquired by a laparoscopic imaging system. Compared with previous studies, the ITS system used here offers straightforward visualization of fluorescence imaging with conventional RGB display by simply toggling a switch since both color RGB and NIR fluorescence imaging are rendered by a processor simultaneously. We first compared the BL-760 fluorescence signals in the cystic duct to those of ICG at a similar postinjection time point. Figure 4 shows representative images acquired from both dyes. After intravenous injection, within 5–10 min, the cystic ducts were successfully visualized in both pigs. As can been seen in Figure 4C, BL-760 shows high TBR (Target-Noise)/(Background-Noise) contrast between the bile duct and the liver parenchyma, compared to ICG, with useful TBR at the 9 min post injection timepoint and persisting over the 2 h measurement. Of note, none of the animals in this study suffered from complications or adverse reactions to the dyes. Specifically, before and after dye injection, we monitored the ECG, beat-per-minute (BPM), oxygen saturation (SpO_2), and tidal volume ($EtCO_2$). The

ECG was consistent during the procedure, monitored BPM was 89 to 90. SpO_2 was measured as 100%. The $EtCO_2$ level stayed between 40 and 45 mmHg.

Cholecystectomy and Model Hepatectomy.

Our next study sought to visualize the gallbladder and cystic ducts in pigs, commonly encountered during laparoscopic cholecystectomies (Figure 5). In doing so, we sought to establish the “Critical View of Safety” criteria set forth for cholecystectomy procedures.[40] One can clearly see the gallbladder and cystic ducts with fluorescence, while the cystic artery is observed in the NIR images with blue color in Figure 5A and B. Relative to liver parenchyma (LP in Figure 5D), extra hepatic ducts (EHD in Figure 5C) are highlighted along with cystic duct and common bile duct.

After careful dissection of the liver hilum, Calot’s triangle (CT in Figure 6B) was exposed and visualized successfully, establishing the “Critical View of Safety”, as depicted in Figure 6A and B. In addition, to demonstrate its usefulness in hepatectomy, we performed left lobectomy in pigs. After liver resection, intrahepatic ducts were exposed and highlighted with fluorescence signals in Figure 6C. While the procedures were performed, small holes in the liver parenchyma were created, and bile leakage (labeled BL) was easily detected in Figure 6C and D.

CONCLUSION

Although other fluorescent dyes have been explored for bile duct visualization, this study is the first to rationally design and test novel NIR dyes for this application.[41-44] There are several distinct advantages of BL-760 relative to the current FDA approved option, ICG. This probe shows superiority in terms of its capacity to function at lower doses of 90 μg/kg and a much shorter time to biliary excretion as well as having a higher TBR (4.48 at 10 min), compared to the clinically available compound ICG.[45] It should also be noted that the assessment of hepatic perfusion by fluorescence imaging following intravenous injection of ICG cannot be carried out repeatedly because, once ICG is administered, nonischemic regions of the liver emit fluorescence signals that persist for hours. However, due to fast excretion into the biliary tract, BL-760 could be injected multiple times to enhance bile duct contrast relative to the liver.

BL-760 also possesses several promising features for use during a range of hepatic surgeries, including hepatectomies. It can differentiate the Glisson from the hepatic vein, and, potentially, also reduce unintended bleeding from small veins. In the case of hepatic duct anomalies, surgeons could identify unexpected biliary tract anatomy. Additionally, this molecule could be used to readily assess bile leakage, which is a serious complication of various hepato-pancreato-biliary surgical procedures.[10] While ICG can be used in this context, this was only possible via intrabiliary infusion after hepatic resection through a transcystic catheter.[20,46] However, using BL-760, no catheterization or retrograde injection are needed due to the fast excretion into the biliary system. This also enables early detection of bile leaks, which should help to prevent liver failure during a living donor hepatectomy. In addition, due to the hampered visibility and inability to palpate the liver surface during laparoscopic or robotic surgery for hepatobiliary system, BL-760 could be of value during

minimally invasive liver surgery.[17] Of note, BL-760 has excitation and emission spectra that are similar to those of ICG, making it ideally suited for existing robot-assisted surgery systems without alteration.[47] Finally, ICG and several related dyes exhibit remarkably selective uptake in certain solid tumor classes, particularly those of hepatic origin, and efforts to characterize the tumor avidity of BL-760 are underway.[48-50] Although additional studies are needed prior to clinical evaluation, BL-760 has promising features for use as a probe of biliary anatomy during various hepatic procedures.

Supplementary Material

Refer to Web version on PubMed Central for supplementary material.

ACKNOWLEDGMENTS

We thank Tracy Thiels and Michael Barnett for assistance with the animal studies. This work was supported by the National Institutes of Health (Center for Cancer Research to M.J.S.), and Sheikh Zayed Institute for Pediatric Surgical Innovation and InTheSmart USA to J.C.

REFERENCES

(1). Cha J; Broch A; Mudge S; Kim K; Namgoong J-M; Oh E; Kim P Real-time, label-free, intraoperative visualization of peripheral nerves and micro-vasculatures using multimodal optical imaging techniques. Biomed. Opt. Express 2018, 9 (3), 1097–1110. [PubMed: 29541506]

(2). Saad N; Darcy M Iatrogenic bile duct injury during laparoscopic cholecystectomy. Tech Vasc Interv Radiol 2008, 11 (2), 102–10. [PubMed: 18922455]

(3). Huang Q; Yao HH; Shao F; Wang C; Hu YG; Hu S; Qiu LJ Analysis of risk factors for postoperative complication of repair of bile duct injury after laparoscopic cholecystectomy. Dig. Dis. Sci 2014, 59 (12), 3085–91. [PubMed: 24965185]

(4). Georgiades CP; Mavromatis TN; Kourlaba GC; Kapiris SA; Bairamides EG; Spyrou AM; Kokkinos CN; Spyratou CS; Ieronymou MI; Diamantopoulos GI Is inflammation a significant predictor of bile duct injury during laparoscopic cholecystectomy? Surg Endosc 2008, 22 (9), 1959–64. [PubMed: 18443865]

(5). Mercado MA; Domínguez I Classification and management of bile duct injuries. World journal of gastrointestinal surgery 2011, 3 (4), 43–48. [PubMed: 21528093]

(6). Viste A; Horn A; Ovrebo K; Christensen B; Angelsen JH; Hoem D Bile duct injuries following laparoscopic cholecystectomy. Scand J. Surg 2015, 104 (4), 233–7. [PubMed: 25700851]

(7). Way LW; Stewart L; Gantert W; Liu K; Lee CM; Whang K; Hunter JG Causes and prevention of laparoscopic bile duct injuries: analysis of 252 cases from a human factors and cognitive psychology perspective. Ann. Surg 2003, 237 (4), 460–9. [PubMed: 12677139]

(8). Flum DR; Dellinger EP; Cheadle A; Chan L; Koepsell T Intraoperative cholangiography and risk of common bile duct injury during cholecystectomy. JAMA 2003, 289 (13), 1639–44. [PubMed: 12672731]

(9). Song G-W; Lee S-G; Hwang S; Sung G-B; Park K-M; Kim K-H; Ahn C-S; Moon D-B; Ha T-Y; Kim B-S; Moon K-M; Jung D-H Preoperative evaluation of biliary anatomy of donor in living donor liver transplantation by conventional nonenhanced magnetic resonance cholangiography. Transplant Int. 2007, 20 (2), 167–173.

(10). Sultan AM; Salah T; Elshobary MM; Fathy OM; Elghawalby AN; Yassen AM; Elmorshedy MA; Elsadany MF; Shiha UA; Wahab MA Biliary complications in living donor right hepatectomy are affected by the method of bile duct division. Liver Transplantation 2014, 20 (11), 1393–1401. [PubMed: 25060964]

(11). Khan OA; Balaji S; Branagan G; Bennett DH; Davies N Randomized clinical trial of routine on-table cholangiography during laparoscopic cholecystectomy. Br. J. Surg 2011, 98 (3), 362–7. [PubMed: 21254008]

(12). White TT; Hart MJ Cholangiography and small duct injury. Am. J. Surg 1985, 149 (5), 640–3. [PubMed: 3993846]

(13). Kruskal JB; Kane RA Intraoperative US of the Liver: Techniques and Clinical Applications. RadioGraphics 2006, 26 (4), 1067–1084. [PubMed: 16844932]

(14). Rosenthal EL; Warram JM; Bland KI; Zinn KR The status of contemporary image-guided modalities in oncologic surgery. Ann. Surg 2015, 261 (1), 46–55. [PubMed: 25599326]

(15). Garland M; Yim JJ; Bogyo M A Bright Future for Precision Medicine: Advances in Fluorescent Chemical Probe Design and Their Clinical Application. Cell Chem. Biol 2016, 23 (1), 122–36. [PubMed: 26933740]

(16). Owens EA; Lee S; Choi J; Henary M; Choi HS NIR fluorescent small molecules for intraoperative imaging. Wiley Interdiscip Rev. Nanomed Nanobiotechnol 2015, 7 (6), 828–38. [PubMed: 25645081]

(17). Verbeek FP; van der Vorst JR; Schaafsma BE; Hutteman M; Bonsing BA; van Leeuwen FW; Frangioni JV; van de Velde CJ; Swijnenburg RJ; Vahrmeijer AL Image-guided hepatopancreatobiliary surgery using near-infrared fluorescent light. J. Hepatobiliary Pancreat Sci 2012, 19 (6), 626–37. [PubMed: 22790312]

(18). Baiocchi GL; Diana M; Boni L Indocyanine green-based fluorescence imaging in visceral and hepatobiliary and pancreatic surgery: State of the art and future directions. World J. Gastroenterol 2018, 24 (27), 2921–2930. [PubMed: 30038461]

(19). Terasawa M; Ishizawa T; Mise Y; Inoue Y; Ito H; Takahashi Y; Saiura A Applications of fusion-fluorescence imaging using indocyanine green in laparoscopic hepatectomy. Surg Endosc 2017, 31 (12), 5111–5118. [PubMed: 28455774]

(20). Kaibori M; Ishizaki M; Matsui K; Kwon AH Intraoperative indocyanine green fluorescent imaging for prevention of bile leakage after hepatic resection. Surgery 2011, 150 (1), 91–8. [PubMed: 21514613]

(21). Pesce A; Latteri S; Barchitta M; Portale TR; Di Stefano B; Agodi A; Russello D; Puleo S; La Greca G Near-infrared fluorescent cholangiography - real-time visualization of the biliary tree during elective laparoscopic cholecystectomy. Hpb 2018, 20 (6), 538–545. [PubMed: 29292071]

(22). Hutteman M; van der Vorst JR; Mieog JS; Bonsing BA; Hartgrink HH; Kuppen PJ; Lowik CW; Frangioni JV; van de Velde CJ; Vahrmeijer AL Near-infrared fluorescence imaging in patients undergoing pancreaticoduodenectomy. Eur. Surg. Res 2011, 47 (2), 90–7. [PubMed: 21720166]

(23). Diana M; Usmaan H; Legner A; Yu-Yin L; D'Urso A; Halvax P; Nagao Y; Pessaux P; Marescaux J Novel laparoscopic narrow band imaging for real-time detection of bile leak during hepatectomy: proof of the concept in a porcine model. Surg Endosc 2016, 30 (7), 3128–32. [PubMed: 26487207]

(24). Buddingh KT; Nieuwenhuijs VB; van Buuren L; Hulscher JB; de Jong JS; van Dam GM Intraoperative assessment of biliary anatomy for prevention of bile duct injury: a review of current and future patient safety interventions. Surg Endosc 2011, 25 (8), 2449–61. [PubMed: 21487883]

(25). Matsui A; Tanaka E; Choi HS; Winer JH; Kianzad V; Gioux S; Laurence RG; Frangioni JV Real-time intra-operative near-infrared fluorescence identification of the extrahepatic bile ducts using clinically available contrast agents. Surgery 2010, 148 (1), 87–95. [PubMed: 20117813]

(26). Cha J; Nani RR; Luciano MP; Broch A; Kim K; Namgoong J-M; Kulkarni RA; Meier JL; Kim P; Schnermann MJ A Chemically Stable Fluorescent Marker of the Ureter. Bioorg. Med. Chem. Lett 2018, 28, 2741. [PubMed: 29510880]

(27). Zheng C; Lau LW; Cha J Dual-display laparoscopic laser speckle contrast imaging for real-time surgical assistance. Biomed. Opt. Express 2018, 9 (12), 5962–5981. [PubMed: 31065406]

(28). Rosenthal EL; Warram JM; de Boer E; Chung TK; Korb ML; Brandwein-Gensler M; Strong TV; Schmalbach CE; Morlandt AB; Agarwal G; Hartman YE; Carroll WR; Richman JS; Clemons LK; Nabell LM; Zinn KR Safety and Tumor Specificity of Cetuximab-IRDye800 for Surgical Navigation in Head and Neck Cancer. Clin. Cancer Res 2015, 21 (16), 3658–66. [PubMed: 25904751]

(29). Gao RW; Teraphongphom N; de Boer E; van den Berg NS; Divi V; Kaplan MJ; Oberhelman NJ; Hong SS; Capes E; Colevas AD; Warram JM; Rosenthal EL Safety of panitumumab-

IRDye800CW and cetuximab-IRDye800CW for fluorescence-guided surgical navigation in head and neck cancers. Theranostics 2018, 8 (9), 2488–2495. [PubMed: 29721094]

(30). Hoogstins CE; Tummers QR; Gaarenstroom KN; de Kroon CD; Trimbos JB; Bosse T; Smit VT; Vuyk J; van de Velde CJ; Cohen AF; Low PS; Burggraaf J; Vahrmeijer AL A Novel Tumor-Specific Agent for Intraoperative Near-Infrared Fluorescence Imaging: A Translational Study in Healthy Volunteers and Patients with Ovarian Cancer. Clin. Cancer Res 2016, 22 (12), 2929–38. [PubMed: 27306792]

(31). Nani RR; Shaum JB; Gorka AP; Schnermann MJ Electrophile-Integrating Smiles Rearrangement Provides Previously Inaccessible C4′-*O*-Alkyl Heptamethine Cyanine Fluorophores. Org. Lett 2015, 17 (2), 302–305. [PubMed: 25562683]

(32). Sato K; Nagaya T; Nakamura Y; Harada T; Nani RR; Shaum JB; Gorka AP; Kim I; Paik CH; Choyke PL; Schnermann MJ; Kobayashi H Impact of C4'-O-Alkyl Linker on in Vivo Pharmacokinetics of Near-Infrared Cyanine/Monoclonal Antibody Conjugates. Mol. Pharmaceutics 2015, 12 (9), 3303–11.

(33). Cha J; Nani RR; Luciano MP; Kline G; Broch A; Kim K; Namgoong JM; Kulkarni RA; Meier JL; Kim P; Schnermann MJ A chemically stable fluorescent marker of the ureter. Bioorg. Med. Chem. Lett 2018, 28 (16), 2741–2745. [PubMed: 29510880]

(34). ChemDraw 18.0; Perkin Elmer, 2018.

(35). Shinohara H; Tanaka A; Kitai T; Yanabu N; Inomoto T; Satoh S; Hatano E; Yamaoka Y; Hirao K Direct measurement of hepatic indocyanine green clearance with near-infrared spectroscopy: separate evaluation of uptake and removal. Hepatology 1996, 23 (1), 137–44. [PubMed: 8550033]

(36). Cusin F; Azevedo LF; Bonnaventure P; Desmeules J; Daali Y; Pastor CM Hepatocyte Concentrations of Indocyanine Green Reflect Transfer Rates Across Membrane Transporters. Basic Clin. Pharmacol. Toxicol 2017, 120 (2), 171–178. [PubMed: 27623731]

(37). Huang LY; Vore M Multidrug resistance P-glycoprotein 2 is essential for the biliary excretion of indocyanine green. Drug Metab. Dispos 2001, 29 (5), 634–637. [PubMed: 11302927]

(38). Gorka AP; Nani RR; Schnermann MJ Harnessing Cyanine Reactivity for Optical Imaging and Drug Delivery. Acc. Chem. Res 2018, 51 (12), 3226–3235. [PubMed: 30418020]

(39). Usama SM; Lin CM; Burgess K On the Mechanisms of Uptake of Tumor-Seeking Cyanine Dyes. Bioconjugate Chem. 2018, 29 (11), 3886–3895.

(40). Vettoretto N; Saronni C; Harbi A; Balestra L; Taglietti L; Giovanetti M Critical view of safety during laparoscopic cholecystectomy. JSLS 2011, 15 (3), 322–5. [PubMed: 21985717]

(41). Figueiredo JL; Siegel C; Nahrendorf M; Weissleder R Intraoperative near-infrared fluorescent cholangiography (NIRFC) in mouse models of bile duct injury. World J. Surg 2010, 34 (2), 336–43. [PubMed: 20033407]

(42). Tanaka E; Choi HS; Humblet V; Ohnishi S; Laurence RG; Frangioni JV Real-time intraoperative assessment of the extrahepatic bile ducts in rats and pigs using invisible near-infrared fluorescent light. Surgery 2008, 144 (1), 39–48. [PubMed: 18571583]

(43). Ashitate Y; Stockdale A; Choi HS; Laurence RG; Frangioni JV Real-time simultaneous near-infrared fluorescence imaging of bile duct and arterial anatomy. J. Surg. Res 2012, 176 (1), 7–13. [PubMed: 21816414]

(44). van den Bos J; Al-Taher M; Hsien SG; Bouvy ND; Stassen LP Near-infrared fluorescence laparoscopy of the cystic duct and cystic artery: first experience with two new preclinical dyes in a pig model. Surg Endosc 2017, 31, 4309. [PubMed: 28271266]

(45). Boogerd LSF; Handgraaf HJM; Huurman VAL; Lam HD; Mieog JSD; van der Made WJ; van de Velde CJH; Vahrmeijer AL The Best Approach for Laparoscopic Fluorescence Cholangiography: Overview of the Literature and Optimization of Dose and Dosing Time. Surg Innov 2017, 24 (4), 386–396. [PubMed: 28457194]

(46). Sakaguchi T; Suzuki A; Unno N; Morita Y; Oishi K; Fukumoto K; Inaba K; Suzuki M; Tanaka H; Sagara D; Suzuki S; Nakamura S; Konno H Bile leak test by indocyanine green fluorescence images after hepatectomy. Am. J. Surg 2010, 200 (1), e19–23. [PubMed: 20637329]

(47). Ishizawa T; Saiura A; Kokudo N Clinical application of indocyanine green-fluorescence imaging during hepatectomy. Hepatobiliary Surg Nutr 2016, 5 (4), 322–8. [PubMed: 27500144]

(48). Ishizawa T; Masuda K; Urano Y; Kawaguchi Y; Satou S; Kaneko J; Hasegawa K; Shibahara J; Fukayama M; Tsuji S; Midorikawa Y; Aburatani H; Kokudo N Mechanistic Background and Clinical Applications of Indocyanine Green Fluorescence Imaging of Hepatocellular Carcinoma. Ann. Surg Oncol 2014, 21 (2), 440–448. [PubMed: 24254203]

(49). Yokoyama N; Otani T; Hashidate H; Maeda C; Katada T; Sudo N; Manabe S; Ikeno Y; Toyoda A; Katayanagi N Real-time detection of hepatic micrometastases from pancreatic cancer by intraoperative fluorescence imaging Preliminary results of a prospective study. Cancer 2012, 118 (11), 2813–2819. [PubMed: 21990070]

(50). van der Vorst JR; Schaafsma BE; Hutteman M; Verbeek FPR; Liefers GJ; Hartgrink HH; Smit VTHBM; Lowik CWGM; van de Velde CJH; Frangioni JV; Vahrmeijer AL Near-infrared fluorescence-guided resection of colorectal liver metastases. Cancer 2013, 119 (18), 3411–3418. [PubMed: 23794086]

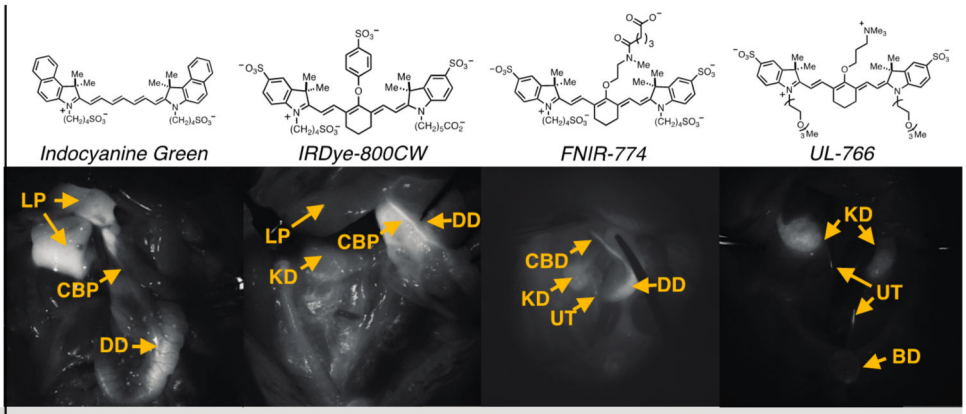

	Indocyanine Green	IRDye-800CW	FNIR-774	UL-766
Net Charge	-1	-4	-4	0
# of Charges	3	6	6	4
CLogP	6.17	2.09	-0.33	-2.43
Bile Excretion (time to max)	++ (4 h)	+ (5 min)	+ (5 min)	---
Specificity (Biliary:Urinary)	100:0	60:40	60:40	5:95

Figure 1.

Comparison of four different previously known heptamethine cyanines. Images shown of rat abdomen 10 min following injection. Description of properties: Net charge, net charge at neutral pH; # of Charges, number of charged functional groups at neutral pH; CLogP, calculated using sodium and chloride counterions.[34] Excretion to biliary tract: + +, high excretion into the bile (CLR > 3); +, low excretion into bile (CLR < 3); −−−, no detectable bile signal and time to maximal detectable signal. CLR, ratio of common bile duct to liver fluorescence signal. Specificity: ratio of biliary and urinary signals at 10 min time point. Yellow arrows: CA = cystic artery, GB = gallbladder, CD = cystic duct, CBD = common bile duct, LP = liver parenchyma, EHD = extrahepatic duct, KD = kidney, UT = ureter, DD = duodenum.

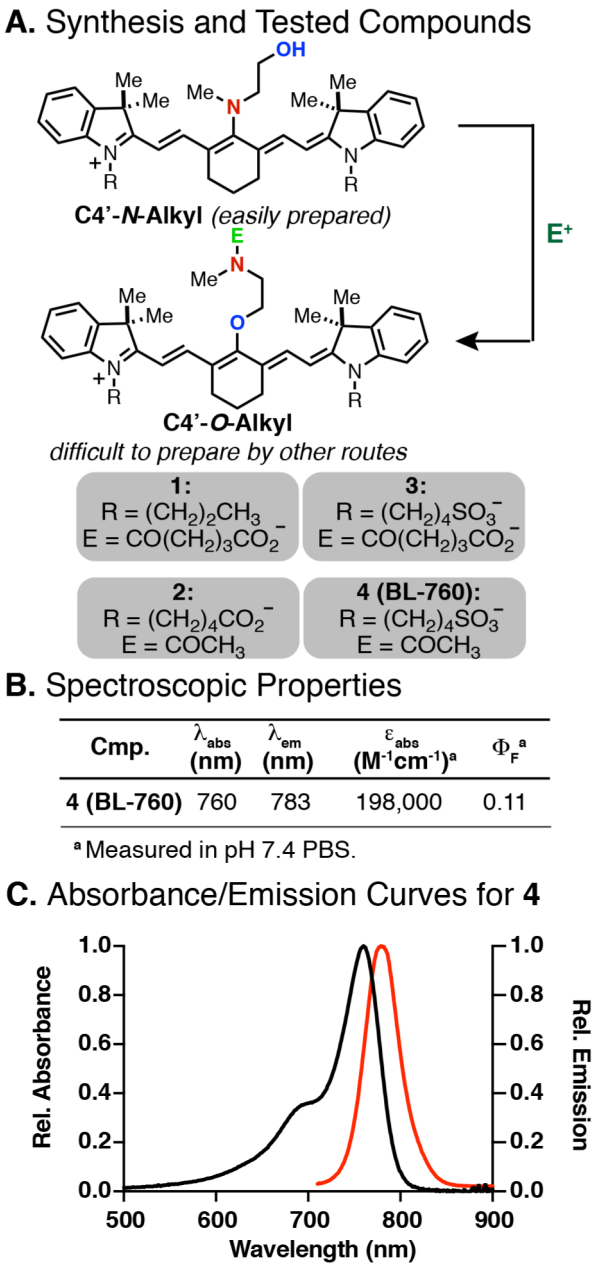

Figure 2.

(A) General synthetic route to C4′-*O*-alkyl cyanines and tested compounds **1–4**, (B) optical properties and (C) absorbance and emission curves for **4**.

Structure	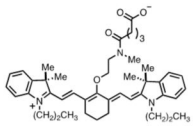 1	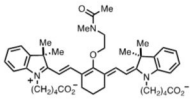 2	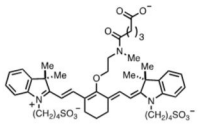 3	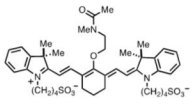 4 *BL-760*
10 min Post-injection	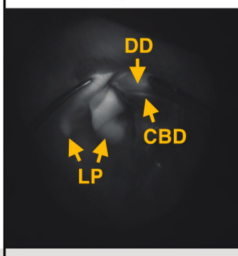	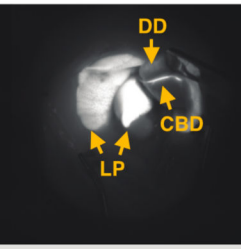	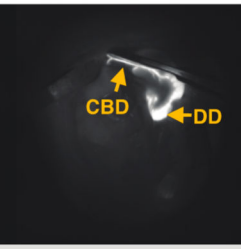	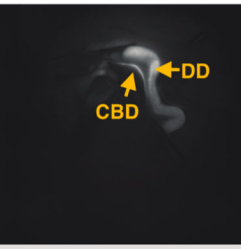
Net Charge	0	-1	-2	-1
# of Charges	2	3	4	3
CLogP	7.66	5.62	3.61	3.83
Bile Excretion (time to max)	+ (45 min)	+ (30 min)	++ (5 min)	++ (5 min)
Specificity (Biliary:Urinary)	100:0	100:0	100:0	100:0

Figure 3.

Comparison of four different C4′-*O*-alkyl heptamethine cyanines with parameters identical to Figure 1.

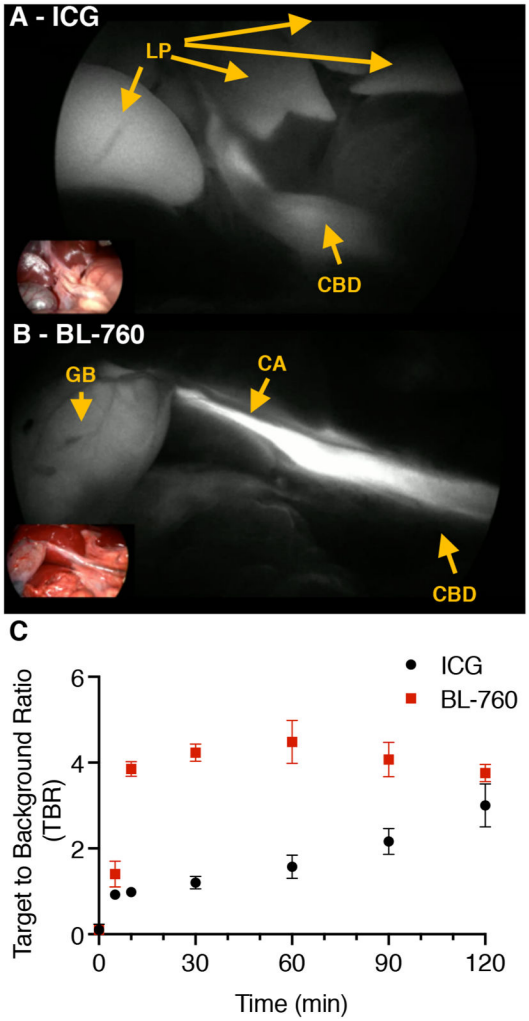

Figure 4.

Comparison between (A) ICG and (B) BL-760 cystic duct images. Arrows: LP = liver parenchyma, CA = cystic artery, GB = gallbladder, CBD = common bile duct. (C) Target-to-background ratio over time using ICG and BL-760 in pigs ($n = 2$).

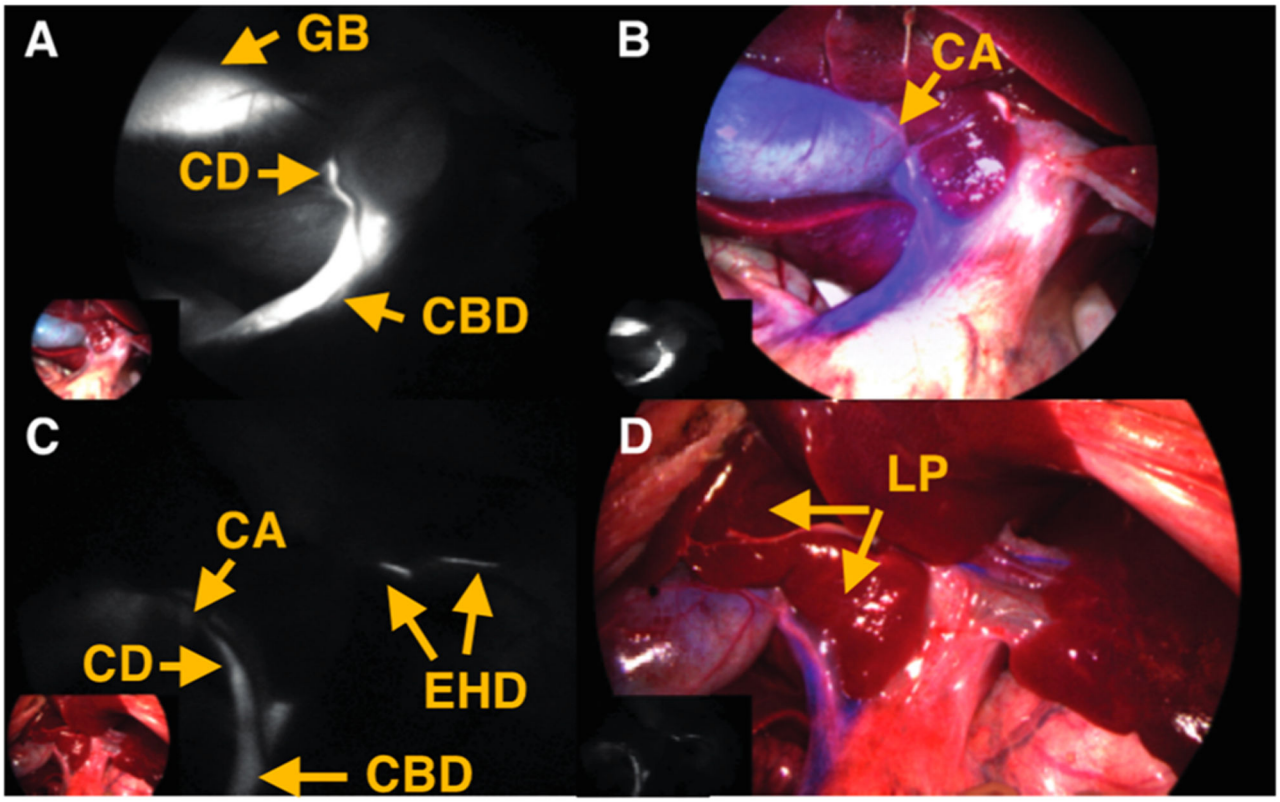

Figure 5.

Postinjection of BL-760 in pigs. (A) NIR fluorescence. (B) Fused image of the first pig study. (C) NIR fluorescence. (D) Fused image of the second pig study. Yellow arrows: CA = cystic artery, GB = gallbladder, CD = cystic duct, CBD = common bile duct, LP = liver parenchyma, EHD = extrahepatic duct.

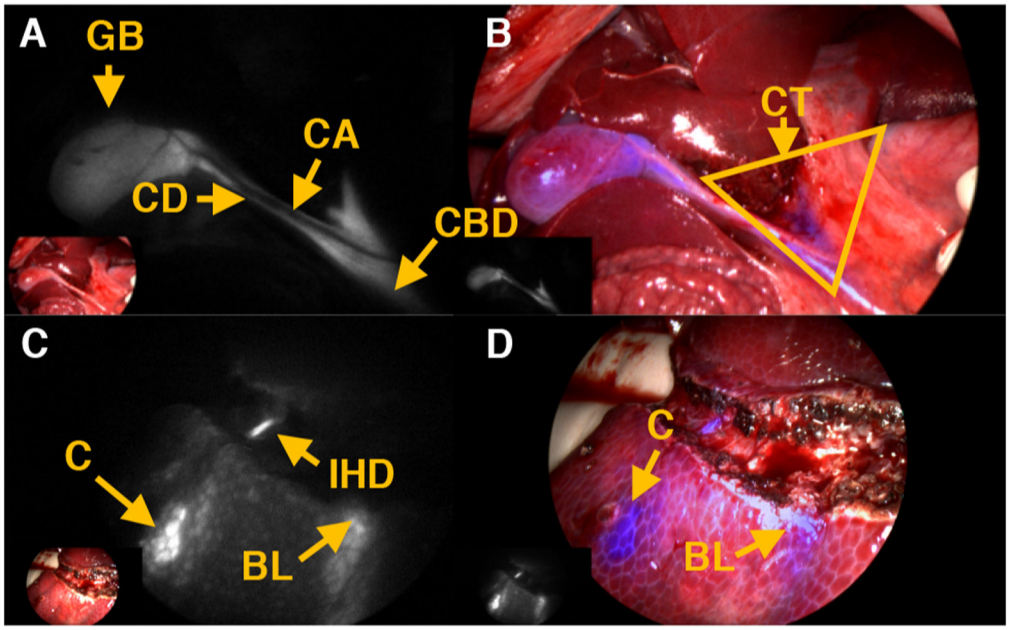

Figure 6.

(A, B) Dissection of the liver hilum and liver resection surgery. (C, D) Critical view of safety (Calot's triangle). Representative images of left lobectomy. Yellow arrows: CT = Calot's triangle, GB = gallbladder, CD = cystic duct, CA = cystic artery, CBD = common bile duct, C = contusion, IHD = intrahepatic duct, BL = bile leaks.